

Static and dynamic conductivity of warm dense matter within a density-functional approach: Application to aluminum and gold

M. W. C. Dharma-wardana*

Institute of Microstructural Sciences, National Research Council of Canada, Ottawa, Canada K1A 0R6

(Received 13 May 2005; revised manuscript received 8 November 2005; published 3 March 2006)

The conductivity $\sigma(\omega)$ of dense Al and Au plasmas is considered where all the needed inputs are obtained from density-functional theory (DFT). These calculations involve a self-consistent determination of (i) the equation of state and the ionization balance, (ii) evaluation of the ion-ion and ion-electron pair-distribution functions, (iii) determination of the scattering amplitudes, and finally the conductivity. We present results for Al and Au for compressions 0.1–2.0, and in the temperature range $T=0.1–10$ eV. Excellent agreement with recent first-principles calculations using multi-ion density-functional molecular dynamics is obtained where the data fields overlap. We review first-principles approaches to the optical conductivity, including many-body perturbation theory, molecular-dynamics evaluations, and simplified time-dependent DFT. The modification to the Drude conductivity in the presence of shallow bound states in typical Al plasmas is examined and numerical results are given at the level of the Fermi Golden Rule and an approximate time-dependent DFT.

DOI: [10.1103/PhysRevE.73.036401](https://doi.org/10.1103/PhysRevE.73.036401)

PACS number(s): 52.25.Mq, 05.30.Fk, 71.45.Gm

I. INTRODUCTION

The static conductivity of matter in the plasma state can be calculated with some confidence, at least for a number of “simple” plasmas, using entirely first-principles approaches [1–4]. Comparisons with experiments are available for a wide range of conditions, at least for Al plasmas [5,6]. Another transport property of great current interest [4,7] is the frequency-dependent conductivity $\sigma(\omega)$. Optical probes provide a convenient diagnostic tool for this plasma conductivity, and some common laser-probe wavelengths, e.g., 300–800 nm, become the window of interest. In fact, many experiments on laser-plasma interactions related to inertial fusion have concentrated on frequency tripled light, 3ω , 351 nm (with the fundamental ω at 1 μm from glass lasers) while there is also current interest in the 2ω (527 nm) regime as an option for indirect-drive ignition [8]. Normally, if the probe frequency is less than the plasma frequency, the probe photons fail to enter the material and only weakly ionized systems can be accessed. However, the recent development of extremely thin (“nanoscale”) plasma-slab techniques [9], known as idealized-slab plasmas [10], has made it possible to study dense plasmas even with low-frequency probes, both in transmission and in reflectivity.

Density-functional calculations of plasma properties are of two types. The first type depends heavily on molecular dynamics (MD) simulations, e.g., Car-Parrinello methods, and treats *only the electrons* via Kohn-Sham theory, while the ion subsystem, explicitly represented by a convenient number N (of the order of $\sim 32–256$) of ions, is made to evolve in time and an average over millions of configurations is taken [11,12]. In full quantum Monte Carlo (QMC) simulations [13,14], even Kohn-Sham theory is not used and hence full QMC is not practical for typical plasma problems. The second type of density-functional theory (DFT) is typi-

fied by our approach where both *electrons and ions* are treated by DFT, so that both subsystems are described by two coupled “single-electron” and “single-ion,” Hartree-like Kohn-Sham equations. The many-body effects (i.e., many-electron and many-ion effects) are included through the exchange-correlation or correlation potentials. This allows an enormous simplification in the numerical work. These equations may be further reduced to extremely simplified Thomas-Fermi approaches yielding approximate results for plasma properties, which are hopefully within an order of magnitude of the more refined results [15].

The general optical conductivity problem is essentially the same as that of opacity calculations for warm dense matter [16]. However, here we approach it from the static-conductivity ($\omega=0$) regime, and take account of any shallow bound states which may exist. The static conductivity provides an evaluation of the dynamic conductivity near $\omega=0$ via the basic Drude formula which assumes a constant relaxation time τ , taken to be the *static* collision time $\tau(0)$. Hence our task can be stated as follows:

1. Calculation of the static resistivity. This involves the following steps: (a) Calculate the Kohn-Sham atom in an electron gas of density n ; (b) use the Kohn-Sham results to form pseudopotentials V_{ie} and scattering cross sections at the given density ρ and temperature T ; (c) use the V_{ie} to form pair potentials and pair-distribution functions; (d) calculate the equation of state (EOS), ionization balance, etc., to obtain effective ionic charges \bar{Z} , electron density $n=\rho\bar{Z}$, etc., and self-consistently, repeating from item (a); (e) calculate the static resistivity and the static relaxation time $\tau(0)$ using, e.g., a Ziman-type formula valid for strong coupling and finite T .

2. Use the energy-level structure of the Kohn-Sham atom to approximately set up bound-bound or bound-free processes which fall within the range of frequency ω considered.

3. Construct the dynamic conductivity $\sigma^0(\omega)$. This yields results equivalent to the Fermi golden rule.

*Email address: chandre.dharma-wardana@nrc.ca

4. Extend the calculation of $\sigma(\omega)$ using time-dependent density-functional theory (TDFT) [16].

While some aspects of this program can be carried out, it is fair to say that a complete, consistent theory of the transport properties of such many-body systems as posed by warm dense matter (WDM), or indeed, even the static properties as embodied in the equation of state *for some regimes of density and temperature* are open to debate, even for well studied systems like aluminum [17], and hydrogen [18]. The objective of the present study is to calculate the static and dynamic conductivity for a number of compressions and densities in the WDM range where the Drude theory may need correction due to the presence of shallow bound states. Such bound states ionize when the compression or temperature is changed, and produce distinctive changes in transport properties. Sharply rising static resistivities under a change of compression are a common feature of some of the theoretical results shown here. However, the establishment of a genuine phase transition requires more care [2]. The $\sigma(\omega)$ of expanded liquid metals and plasmas show [19] effects arising from clustering and excitonic effects, as the metal-insulator transition is approached. These excitonic effects are not important in dense systems. While Al has been an object of extensive study, recent experiments in the warm dense matter regime have focused on gold targets [20,21]. Here we present numerical results for Al and Au for conditions typical of warm-dense matter.

II. STATIC RESISTIVITY

We use atomic units (Hartree=1 a.u., with $|e|=\hbar=m_e=1$). A direct approach to the conductivity via Green's-function perturbation theory for the current-current propagator has not been successful even for simple metallic solids. The Ziman formula based on a variational approach to the Boltzmann equation has been more successful. Instead of the Boltzmann equation with its many assumptions, we approach the Ziman formula and the Kubo-Greenwood formula as essentially forms of the Fermi golden rule, and provide the needed inputs from DFT.

A. Description of the plasma using the Kohn-Sham equations

We use the Kohn-Sham technique, and construct the non-linear charge density around a *single* nucleus immersed in the plasma containing other ions and electrons. The nucleus and its charge cloud $n(r)$ of bound states and continuum-electron states constitute a neutral object. This neutral object is called the *neutral pseudoatom* (NPA), following the usage of e.g., Ziman and Dagens [22]. A part of $n(r)$ arises from the free electrons and is denoted by $n_f(r)$. This $n(r)$ and $n_f(r)$ depend on the mean density n of the electron fluid, the temperature T , and the nuclear charge Z . For large r , far away from the nucleus, $n_f(r) \rightarrow n$, the mean electron density. The Kohn-Sham procedure leading to the NPA provides the phase shifts of the continuum electrons when they scatter from the nuclei. These satisfy the Friedel sum rule, and are used for constructing the scattering cross sections (or pseudopotentials) which describe the electron-ion interaction. The

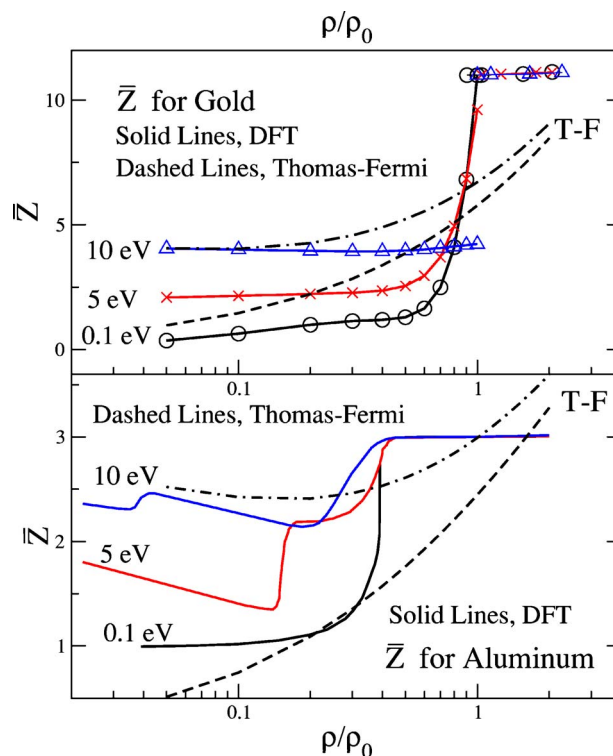


FIG. 1. (Color online) Effective ionic charge \bar{Z} of warm dense gold and aluminum as a function of the compression for several temperatures. The Thomas-Fermi estimates (dashed lines) at $T = 10$ eV and 0.1 eV are also shown.

pseudopotential has an effective ionic charge \bar{Z} and behaves as $-\bar{Z}/r$ for large r . For ions in free space $\bar{Z}=Z-n_b$, where n_b is the number of bound electrons at the nucleus. The situation is more complicated in a plasma. The electrons near an ion in a plasma are bound by the nucleus as well as the cavitylike ionic-charge depletion associated with the ion-ion pair-distribution function $g_{ii}(r)$, as discussed in Ref. [23]. Thus \bar{Z} is strictly a Lagrange multiplier which enables a formal separation between the bound electrons and delocalized electrons in the system while satisfying the Friedel sum rule and ensuring charge neutrality by $\rho=n/\bar{Z}$. Here ρ is the mean nuclear density or, equivalently, the mean ion density. This separation is not simple if there are localized continuum resonances, etc. For details we refer to our previous work [2,23,24]. A plot of the effective charge \bar{Z} for Al and Au for WDM conditions is given in Fig. 1, together with an estimate from Thomas-Fermi theory [15]. For Al, the sharp rise of \bar{Z} to 3 occurs near an ion compression of $\kappa \sim 0.4$, while Kuhlbrodt *et al.* [27], using a “chemical” approach, display (see their Fig. 1) an upturn near a mass density of ~ 0.6 g/cm³, i.e., $\kappa \sim 0.2$. Similarly, their concentration fractions x_i are in general different from what we have reported in our calculations [2], a sample of which is given in Table I. The sharp rise in Au arises only very close to unit compression, when all 10 *d*-shell electrons become delocalized, leading to a theoretical resistivity of $27 \mu\Omega$ cm for liquid Au at the melting point, in good agreement with the experimental value of $31.2 \mu\Omega$ cm. The experimental resistivity of

TABLE I. Fractional composition x_i of integer-charge state I , i.e., Al^{I+} , $I=0-3$, of Al plasma at $T=1.5$ eV, as a function of the ion compression $\kappa=\rho/\rho_0$ calculated within the full multispecies approach of Ref. [2].

ρ/ρ_0	x_0	x_1	x_2	x_3
0.159	0	0.824	0.172	0
0.312	0	0.804	0.188	0.007
0.348	0.865	0.130	0	0
0.507	0	0.614	0.294	0.092
0.667	0	0	0	1
1.0	0	0	0	1

($25 \mu\Omega \text{ cm}$) for liquid Al at its melting point is also in good agreement with our theoretical value of $25.7 \mu\Omega \text{ cm}$ at 928.4 K .

The pseudopotentials used in many of the solid-state or molecular-code packages [28] have some of the necessary transferability and could be quite useful if the applicable \bar{Z} is available. The codes require that the pseudopotentials be used within a Schrödinger or Kohn-Sham procedure rather than in a linear-response scheme, and hence they cannot be directly used within a Ziman-type formula. They also usually assume $T=0$ exchange-correlation functionals $E_{xc}(n, T=0)$ whereas the temperature effects in $E_{xc}(n, T \neq 0)$ play a crucial role, especially near ionization thresholds [29]. The pseudopotentials assume a single configuration for the core electrons, with a fixed \bar{Z} , e.g., 3 in the Al pseudopotential, whereas the \bar{Z} in WDM is unknown. Also, Fig. 1 shows that \bar{Z} does not interpolate with T in a simple manner, especially for Al. Thus WDM effectively demands the use of all-electron codes. However, a pseudopotential with $\bar{Z}=3$ will work for ionizations smaller than 3 as well. The Vienna-Ab-initio Simulation Package (VASP) has been used by Desjarlais [4,12] and collaborators in recent DFT-MD calculations of low to moderate density warm matter. These provide a very useful input to the available calculations of resistivities and provide comparisons with some experiments (see Fig. 2) and our results. We discuss this type of calculation in Sec. III A.

Sometimes, instead of using an all-electron self-consistent-field method or a suitably constructed pseudopotential, the electron-ion interaction is replaced by a Yukawa-type interaction (effectively, a Debye-screened interaction). This procedure is not justifiable since the energies of bound-state electrons correspond to very high frequencies and there is no screening. Further, the orthogonality of the continuum eigenstates and the bound states ensures that there is very little penetration of the free electrons into the bound-electron region. Thus calculations using a Debye-like potential and “extending” them using, say, T -matrix methods, have no systematic justification [26]. However, some of these models have been investigated by Redmer *et al.* [27]. A number of ion species, energies, etc., are assumed in this “chemical model” and the total free energy is minimized using mass action laws with ideal activities. Born approximations for the

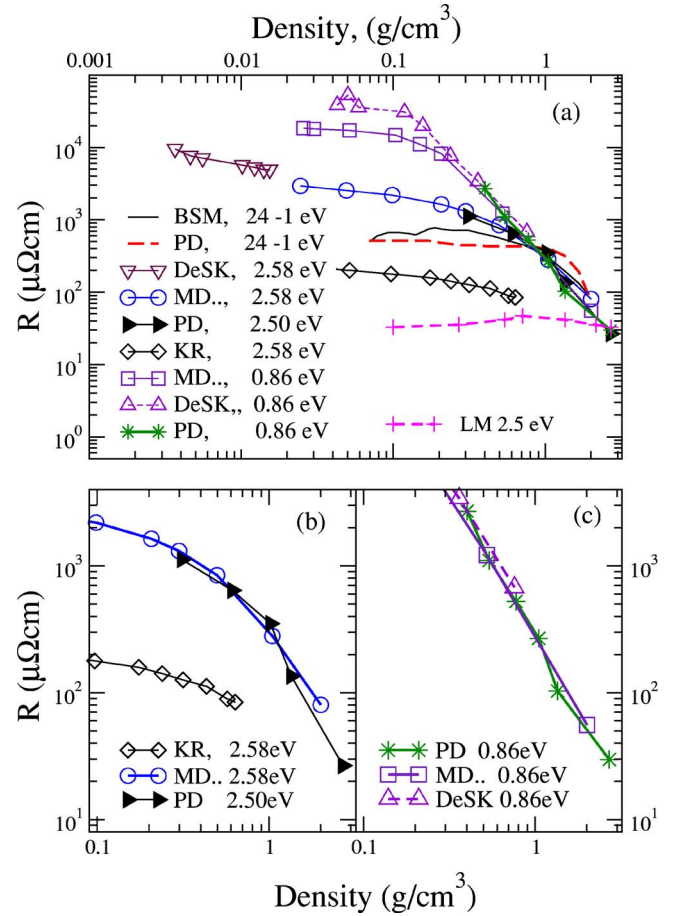


FIG. 2. (Color online) Comparison of experimental and theoretical results for the resistivity of Al plasmas. Panel (a) BSM—experimental results from Ref. [5], Benage *et al.*, T ranges from ~ 24 to 1 eV. Theory, Perrot and Dharma-wardana, labeled PD, Refs. [1,2] are for the BSM range of T ; also at $T=0.86$ eV (10^3 K) and 2.5 eV ($\sim 3 \times 10^3$ K). Selected experimental data of DeSilva *et al.*, Ref. [6] at 10^3 K and 3×10^3 K are labeled DeSK. The DFT molecular-dynamics results of Mazevet *et al.*, labeled MD..., are at 10^3 K and 3×10^3 K. Results from the “chemical” model of Kuhlbrodt *et al.*, KR, Ref. [27]. The Thomas-Fermi model of Lee and More (LM), Ref. [15], is given only at $\sim 3 \times 10^3$ K. Panels (b) and (c) show the excellent agreement between the two first-principles calculations, MD and PD, in the *warm dense matter* range ($\rho > 0.1 \text{ g/cm}^3$), at 10^3 K and 3×10^3 K, respectively.

correlation functions and T -matrices as well as Debye screening are used at various levels of accuracy. Their results [27] usually tend to underestimate the static resistivities (Fig. 2) obtained from first-principles methods, but provide a useful *grosso modo* estimate of the transport properties of a variety of plasmas.

Instead of using Debye/Yukawa-type potentials, it is possible to construct, in many (but not all) situations, a soft, local pseudopotential $V_{ie}(q)$ which is weak in the sense that the non-linear electron-density “pileup” $n_f(r)$, obtained via the Kohn-Sham equation, is recovered within *linear* response theory. That is, we *define* the $V_{ie}(q)$ such that

$$n_f(r) = -V_{ie}(q)\chi(q). \quad (1)$$

Here $\chi(q)$ is the electron linear-response function. This $V_{ie}(q)$ is specific to the electron density n , temperature T , and the atomic number Z . Because \bar{Z} has to be self-consistently determined, our computational codes input the nuclear charge Z , the free-electron density n , and T to first compute the single-nucleus problem in the plasma. Then we construct the multiconfiguration plasma as in Ref. [2], or the single neutral-pseudoatom (NPA) model as in Ref. [24]. The ion density is finally deduced by requiring that $n = \bar{Z}\rho$. Unless otherwise stated, in this study we have used the simpler NPA model. It is often convenient to write the pseudopotential in the form

$$V_{ie}(q) = \bar{Z}M_q v(q), \quad v_q = 4\pi/q^2, \quad (2)$$

where v_q is the bare Coulomb potential and M_q is a form factor. Only a local pseudopotential is used, and this is quite adequate for an analysis of the experimental data currently available. Since the pseudopotential is weak by construction, i.e., because the linear-response form of Eq. (1) is valid, the ion-ion pair potential is

$$U_{ii}(q) = 4\pi\bar{Z}^2/q^2 + |V_{ie}(q)|^2\chi(q). \quad (3)$$

Note that this method of constructing a pair potential cannot be used for hydrogen plasmas. Since the pointlike $1/r$ interaction cannot be treated by linear response, a full Kohn-Sham analysis [23] or a CHNC approach [18] is needed, except at very high temperatures. Hence the results of Reinholz *et al.* [25] who use linear response for the H^+ -electron interaction would be applicable only under very weak-coupling conditions. Given $U_{ii}(q)$, the ion-ion distribution function $g_{ii}(r)$ and the structure factor $S(k)$ can be calculated using the hypernetted-chain (HNC) equation or its extension where a bridge term is included [30]. We note (see below) that the HNC equation (or its extension) is a form of the Kohn-Sham equation for classical particles (here, Al^{z+} or Au^{z+} ions). The Kohn-Sham classical correlation potential can also be approximated by hard-sphere correlations. Such an approximation, equivalent to the use of the Percus-Yevick theory for the structure of the fluid, is useful if the HNC equation based on Eq. (3) fails to converge. In fact, as seen from Fig. 2, the Kohn-Sham/HNC procedure used in our work fails to converge for low densities (unless special effort is taken with optimized grids, continuum resonances, etc.), and hence we present results for $\rho > 0.1$ g/cm³. The single-configuration NPA has to be replaced by a multi-configuration (and possible multicenter) approach for low densities. However, when there is convergence, the computational time for evaluating a resistance from first principles is only a few minutes using a simple workstation. Some of our numerical codes for carrying out these procedures are available via the internet to any interested researcher [31].

B. Is this a “one-center” approach?

To answer this question, we consider the DFT for a two-component system consisting of electrons [density profile

$n(r)$] and ions, with a density profile $\rho(r)$, with respect to an ion positioned at the origin [32]. Then the Hohenberg-Kohn-Mermin theorem states that the free energy $F[n(r), \rho(r)]$ is a functional of the density distributions such that

$$\partial F[n(r), n(r)]/\partial n(r) = 0, \quad (4)$$

$$\partial F[n(r), \rho(r)]/\partial \rho(r) = 0. \quad (5)$$

The first of these equations leads to an effective *single-electron* equation, viz., the Kohn-Sham equation where the effective potential contains an *exchange-correlation potential* which takes account of many-electron effects. The second equation is coupled to the first. It also leads to a Kohn-Sham equation which is a classical equation for a *single ion*. This also contains an ion-ion *correlation potential* which brings in the effects of the multicentered system (there is no exchange since the ions are classical). This ion-correlation potential can be approximated by, e.g., a sum of HNC graphs. Thus the method is firmly rooted in a many-electron, many-ion DFT approach which does *not* invoke the Born-Oppenheimer approximation. Since the theory is based on distribution functions, it is manifestly nonlocal and can be made free of electron self-interaction errors. Our approach may be contrasted with the DFT-MD method of Car-Parrinello (CP) which avoids the need for an ion-correlation potential by an explicit N-ion simulation (while applying DFT only to the electrons). Hence CP demands a much larger computational effort, and ignores the simplifying features present in a relatively dense plasma. Some CP-based calculations (e.g., Refs. [14,33]) have confirmed results obtained by the numerically simpler methods that we have used. Clearly, panels (b) and (c) of Fig. 2 also show that the DFT-MD of Mazevet, Desjarlais *et al.*, and our NPA calculations are in good agreement.

C. Extended Ziman formula for strongly coupled electrons and ions

The original Ziman formula is an application of the Boltzmann equation to liquid metals. It was extended to finite T by a number of authors [34]. The crux of the problem is the evaluation of the collision rate. Compared to some methods well known in plasma theory (e.g., Lenard-Balescu), the collision rate is easily evaluated using the “Fermi golden rule.” We briefly recapitulate Ziman theory in the language of the Fermi golden rule, to bring it into line with the Kubo-Greenwood formula and also self-energy calculations [35,51].

In the relaxation-time approximation, we assume that the perturbed Fermi distribution $f(k)$ for electrons with momentum \vec{k} relaxes toward the equilibrium distribution $f_0(k)$ according to the equation

$$-\left. \frac{\partial f}{\partial t} \right|_{\text{col}} = \frac{f(k) - f_0(k)}{\tau(k)}. \quad (6)$$

Thus the deviation $f_1(k) = f(k) - f_0$ from equilibrium is characterized by the k -dependent parameter set $\tau(k)$. Considering an electron scattered elastically from state \vec{k} to state \vec{k}' , with $|k| = |k'|$, $\epsilon_k = \epsilon_{k'}$, the net scattering rate is the difference of the

two processes $(\vec{k} \rightarrow \vec{k}') - (\vec{k}' \rightarrow \vec{k})$. The initial and final densities of states for the $\vec{k} \rightarrow \vec{k}'$ process is $f(k)$ and $[1 - f(k')]$. Hence the Fermi golden rule gives

$$R(k \rightarrow k') = (2\pi/\hbar) \sum |T_{kk'}|^2 \delta(\epsilon_k - \epsilon_{k'}) f(k) (1 - f(k')),$$

$$R(k' \rightarrow k) = \text{permutation of } k \text{ with } k', \text{ etc.}$$

Since $\epsilon_k = \epsilon_{k'}$, this involves only an angular integration and $|k| = |k'|$. Since the energy is not changed, the static resistivity arises *purely from momentum randomization*. The change in momentum is $q^2 = 2k[1 - \cos(\theta)]$. Here θ is the angle between \vec{k}' and \vec{k} . This $[1 - \cos(\theta)]$ term does not appear in the usual relaxation time, which is the time between scattering events. Using these rates in Eq. (6), we obtain a result for the *inverse* of the transport relaxation time,

$$\frac{1}{\tau(k)} = 2\pi \sum \delta(\epsilon_k - \epsilon_{k'}) |T_{kk'}|^2 [1 - \cos(\theta)]. \quad (7)$$

Here the sum merely indicates the integration over θ . The “ T -matrix” appearing here describes the scattering of an electron by the whole ion distribution (i.e., not just one ion). Given a set of ions at instantaneous positions R_I , then the interaction of an electron at \vec{r} with the whole distribution is of the form

$$V(r) = \sum_I V_{ie}(\vec{r} - \vec{R}_I). \quad (8)$$

The matrix element between the initial state \vec{k} and the final state \vec{k}' , with $\vec{q} = \vec{k}' - \vec{k}$, is

$$V(q) = \sum_I \bar{Z} M_q v_q e^{iq \cdot \vec{R}_I}. \quad (9)$$

Note that

$$\rho_q = \sum_I \exp(i\vec{q} \cdot \vec{R}_I), \quad (10)$$

$$\langle \rho_q \rho_{-q} \rangle = N_i S_{ii}(q). \quad (11)$$

Thus the ion-ion structure factor $S(q)$ and the single-ion scattering cross section (or the pseudopotential) from a single ion combine to give the full scattering T -matrix. The dependence on the structure factor becomes negligible for $T > 10$ eV. The individual scattering cross section can be replaced by a single-center T -matrix (to be denoted by $t_{kk'}$) obtained from the phase shifts of the NPA calculation for a single nucleus. The $S(q)$ is also obtained from the pair potential constructed from the same NPA calculation. In Ref. [1], we showed how to avoid the calculation of the $S(q)$ by directly computing the scattering cross section from the *total ion distribution*. That is, $T_{kk'}$ need not be factored into single-center $t_{kk'}$ and the associated structure factor. Such an approach is needed for *strongly interacting systems* where such a factorization may not be valid. In this context, we note that the resistivities calculated by us using the “single-center” model [i.e., $t_{kk'} S(q)$], and the full ion-distribution model ($T_{kk'}$ for strong scattering) for H plasmas were independently confirmed by

the quantum Monte Carlo simulations of Kwon *et al.* [14]. However, if the pseudopotential is weak, the $S(k)$ and the single-center $t(k)$ may be used.

Given the inverse relaxation time $1/\tau(k)$ for an electron of momentum k , or equivalently, $1/\tau(\epsilon)$ for the energy, $\epsilon = k^2/2$, we need to average this over all the electron energies to obtain a resistivity or a conductivity. The averaging used in the Ziman formula leads to a *resistivity*, while a direct application of the Boltzmann equation would lead to a conductivity. Thus,

$$\sigma = \frac{\omega_p^2}{4\pi} \langle \tau(\epsilon) \rangle, \quad R = \frac{4\pi}{\omega_p^2} \langle 1/\tau(\epsilon) \rangle. \quad (12)$$

The Boltzmann equation shows that the averaging relevant to the conductivity calculation is such that

$$\sigma = \frac{\omega_p^2}{4\pi} \frac{2}{3n_e} \int \frac{d\epsilon}{\pi^2} (\sqrt{2\epsilon^{3/2}})^{-1} \frac{\partial f_0(\epsilon)}{\partial \epsilon} \tau(\epsilon). \quad (13)$$

On the other hand, the averaging over the $1/\tau(\epsilon)$ used in the extended Ziman formula for the resistivity is somewhat different,

$$\langle 1/\tau \rangle = - \int_0^\infty d\epsilon g(\epsilon) \frac{\partial f(\epsilon)}{\partial \epsilon} \tau(\epsilon)^{-1}. \quad (14)$$

Here $g(\epsilon)$ is a density-of states factor which is unity for free noninteracting electrons. It should be constructed from the phase shifts in a strongly scattering environment. If this is not included, phase-shift based calculations and pseudopotential-based calculations of the resistivity would differ significantly [3] even when they should not.

The initial assumption, Eq. (6), was that the modified distribution was defined via a relaxation time. A more complete approach is to represent the modified part $f_1(k)$ as a series expansion in a set of suitably constructed orthogonal polynomials, and obtain a variational solution. The polynomials appropriate for WDM containing degenerate (and partially degenerate) electrons are just those discussed by Allen *et al.* [37]. In the classical limit, such polynomials are the well known Sonine polynomials. The usual relaxation-type approach is equivalent to a single-polynomial solution. This is adequate for dense Al plasmas, and for the range $0 < T < 10$ eV studied here. However, this is probably not so for Al at 1/4 of the normal density, or for lower densities. We have less experience with Au plasmas to assess the quality of the resistivities for Au obtained here. The polynomial representation of $f_1(k)$ is also brought up in relation to e - e interactions, in Sec. II E.

D. Numerical results in the static limit

A comparison of the static resistivities for Al calculated using the above methods was already presented in Fig. 2. A tabulation of the static resistivity of Al in the WDM region is given in Table 1 of Ref. [36], and displayed in Fig. 3 so as to emphasize the rapid rise of the resistivity (for Au, see Fig. 4) toward low densities, masked in commonly used log-log plots. Here we note a number of difficulties in the calcula-

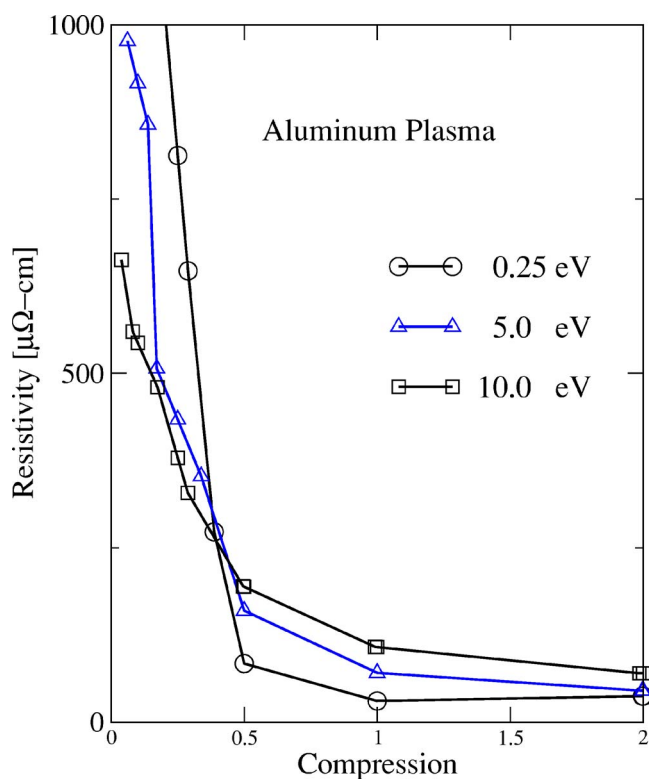


FIG. 3. (Color online) Resistivity of warm dense aluminum as a function of the compression for several temperatures.

tion. If we consider an Al plasma at a compression $\kappa=0.25$, at $T > 2.5$ eV the Al ion has the bound shells $1s$, $2s$, $2p$, and $3s$. The $3s$ level becomes increasingly shallow as the temperature is reduced. Below approximately $T \sim 2.5$ eV, the $3s$ level begins to “evaporate” and becomes free, i.e., the $3s$ bound electrons ionize. Even at 2.5 eV, the occupation of the $3s$ level is ~ 0.744 . The ionization state \bar{Z} increases from ~ 1.667 to 3. The model where we have a single average \bar{Z} is clearly not satisfactory in such a region. The plasma contains an equilibrium mixture of several ionization states Al^{Z_i+} where $Z_i=I$ is an integer, with concentrations x_i such that

$$\bar{Z} = \sum_i x_i Z_i. \quad (15)$$

For such situations (and indeed in general), the concentrations x_i have to be determined from the minimum of the total free energy. Some results for an Al plasma are given in Table I. This shows the limitation of the average atom model, since different species have different excitation spectra and contribute to the dynamic conductivity. The extreme nonlinearity and sharp jumps of a given x_i with the ion compression becomes less nonlinear if examined as a function of the electron compression [2]. At present, no results from VASP-type simulations are available for these fractional compositions x_i of charge states. In fact, VASP calculations do not use intermediate quantities such as the x_i , Z_i , or \bar{Z} . As seen from Fig 1, the situation is somewhat simpler for warm-dense Au. However, if n species of ions are possible, then n different Kohn-Sham equations have to be solved, and $n(n+1)/2$ ion-ion distribution functions have to be determined, and the

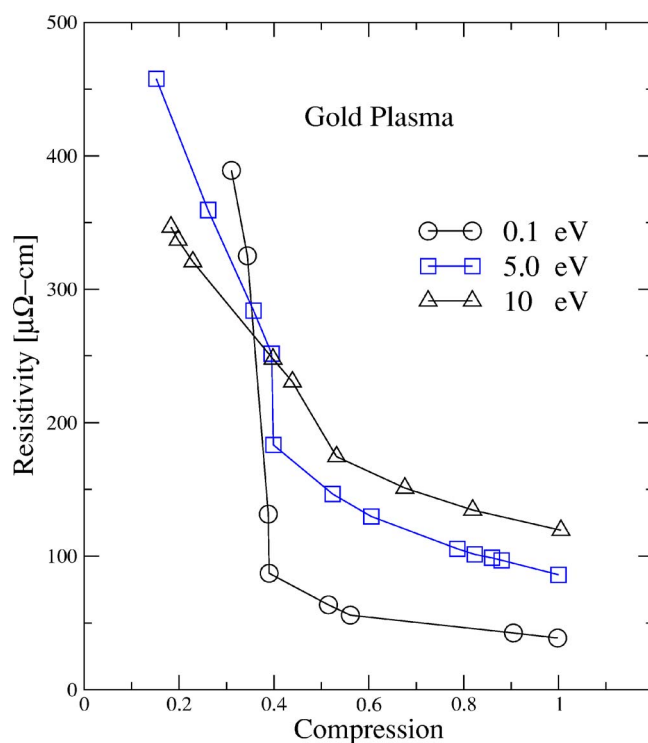


FIG. 4. (Color online) Resistivity of warm dense gold as a function of the compression for several temperatures.

total free energy has to be calculated as a function of n and x_i . The minimum property of the free energy yields the equilibrium plasma conditions from which the resistivity is calculated, using the n scattering cross sections and the $n(n+1)/2$ structure factors. We reported such a calculation for Al in Ref. [2]. Our experience is that, even with a multi-ion fluid model, the self-consistent equations may fail to converge since the $3s$ level (or the $2p$ level) affects the iterative procedure. Majumdar and Kohn have shown that physical properties of a system should be continuous across the region where an electronic state moves from being a bound state to a continuum state [38]. Hence we may calculate the resistivity in two adjacent regions separated by a nonconvergent region, and smoothly join the calculated resistivity across the “difficult” region. In Table II, we show the Kohn-Sham eigenvalues of the bound-electron states for Al ions in various plasmas. Although the Kohn-Sham eigenvalues do not exactly correspond to the excitation energies, they provide an initial estimate which can be improved using the methods of time-dependent density-functional theory, or using self-energy calculations [35]. As the density decreases and the temperature increases, we inevitably pass through regions of T, κ where the problem of bound states which hover near ionization becomes important. In a multicenter approach, e.g., as in a quantum-MD simulation, such states become cluster states. Calculations (e.g., see Table I, Ref. [36]) show that, for $\kappa=0.1$, the resistivity essentially decreases with T , while for $\kappa=0.25$, the resistivity gradually increases in value, goes through a plateaulike region, and then begins to decrease with temperature. The same behavior holds for other higher compressions. Some authors have explained the plateau in the resistivity as indicating a mean free path which

TABLE II. Kohn-Sham energy-level structure for several Al plasmas within the NPA average-configuration model. The energies are in Hartrees.

Level	$\kappa=4$	$\kappa=2$	$\kappa=1$	$\kappa=0.5$	$\kappa=0.25$	$\kappa=0.1$
$T=10$						
\bar{Z}	3.043	3.0166	3.0164	3.0194	2.6060	2.2427
$2p$	-2.9311	-3.5922	-4.1529	-4.6411	-5.1928	-5.8159
$3s$					-0.1871	-0.6168
$3p$						-0.1643
$T=2.5$						
\bar{Z}	3.0427	3.0051	3.0003	3.0000	1.6643	1.6240
$2p$	-2.7838	-3.4422	-3.9268	-4.2875	-4.7055	-4.9258
$3s$					-0.1178	-0.2758
$T=0.1$						
\bar{Z}	3.0437	3.0053	3.0003	3.0000	does not	converge
$2p$	-2.7462	-3.4008	-3.8853	-4.2393	due to	$3s$ level
$3s$					"	"

has become as small as possible (as in the Joffe-Regel rule). We *disagree* with this explanation of the existence of a resistivity plateau in these cases in terms of a saturation of the mean free path. Quantitative agreement is provided with a very *different picture* of what happens in the plasma. As the material is heated, its resistivity increases just as in a metal, due to the increased availability of a strip of states (of width $k_B T$) at the Fermi surface for the “phononlike” scattering to take place. However, as $k_B T$ increases, the number of current-carrying electrons also increases, compensating the resistivity increase. During this process, the chemical potential μ of the plasma electrons begins to decrease, and a temperature $T_{\mu=0}$ is reached when μ passes through zero and toward negative values. Then the Fermi sphere gets broken down, and *all* the electrons, and not just those near the Fermi surface, begin to conduct. The plasma is essentially classical. The resistivity *decreases* as the temperature increases. The plateau defines the transition to the Spitzer-like regime. The Fermi energy of the $\kappa=0.1$ case is small and it is already behaving like a classical plasma. The negativity of the electron chemical potential clearly indicates this feature. The picture is more complicated since the Fermi surface changes not only because of the temperature, but also because the ionization of bound electrons changes the value of \bar{Z} . This pushes the value of $T_{\mu=0}$ and the onset of the plateau to higher temperatures than in a model with constant \bar{Z} . It is easy to allow for this in a calculation of $T_{\mu=0}$ and confirm that the resistivities $R(T, \kappa)$ given in Table I of Ref. [36] (and in Ref. [39]) are consistent with this picture.

E. Contribution to the resistivity from electron-electron scattering

Discussions of the electrical resistivity of plasmas sometimes contain allusions to the electron-electron ($e-e$) contribution to the electrical resistivity [41–43]. It is claimed that

$e-e$ contributions kick in as the electrons lose their degeneracy. However, for uniform systems, the electron-current operator $\vec{j}=(e/m)\vec{k}$ commutes fully with the electron-electron interaction Hamiltonian H_{ee} ,

$$\vec{j}H_{ee} - H_{ee}\vec{j} = 0. \quad (16)$$

This shows that the current is *conserved* under the $e-e$ interaction, and this holds irrespective of the electron degeneracy. Hence electron-electron interactions *cannot* contribute to the resistivity arising from the electron current. The $e-e$ interaction enters indirectly since it screens the electron-ion pseudopotential $V_{e-i}(q)$. That is, electron-ion vertices *must occur in all Feynmann diagrams* which contribute to the resistivity, and no pure $e-e$ interaction terms should occur. In periodic systems, pure $e-e$ scattering occurs through umklapp processes [44] Any theory of the conductivity of a uniform plasma *must* obey the conservation principle of Eq. (12). Plasmas can be considered uniform if there are no density variations within a length scale significantly larger than the mean free path. Classical transport calculations for systems with gradients (i.e., no translational invariance) are well known [45]. The quantum calculation is also well known in transport across heterostructures [46]. Even if the system were not uniform, but contained a quadratic confining potential, Kohn’s theorem [47] ensures that electron-electron interactions play no part in the static or dynamic conductivity. Kohn’s theorem holds at any degeneracy.

The Boltzmann equation contains the displacement $f_1(k) = f(k) - f_0(k)$ of the distribution function from equilibrium. Spitzer and Härn attempted to go beyond the one-parameter model of Eq. (6) by including additional flexibility into $f_1(k)$, and presented physical arguments using the $e-e$ interaction as the motivation. Appel in his first paper [42] follows Spitzer and Härn in its physical picture, but somewhat modifies his stance in the second paper [42]. In the work of Röpke *et al.* [43], Zubarev’s quasiequilibrium density operator is used with a moment expansion using a set of “macroscopic non-equilibrium states” P_m . The choice of such P_m within Zubarev’s approach is an open question. The moment expansion assumes short-ranged potentials. Röpke *et al.* have chosen a set of P_m to reproduce the Spitzer-Härn result in the weakly interacting “Spitzer limit.” However, this does not establish the validity of results of the Spitzer-Härn type.

A completely uniform classical one-component plasma of electrons has no finite linear-response resistivity, in spite of the electron-electron interaction. If we look at the low-density experimental results for electron-ion plasmas presented in Fig. 2, we see that relatively good agreement is obtained within the DFT-MD simulations of Mazevet *et al.*, and these *do not* contain the $e-e$ contributions proposed by, say, Röpke *et al.* and others [42]. Thus the direct role of electron-electron interactions, taken for granted in the plasma literature, needs to be seriously reconsidered.

III. DYNAMIC CONDUCTIVITY

The static conductivity includes only elastic scattering processes. If the effects of interactions and bound states are

small, the conductivity of “free” electrons driven by an external field $E_0 \cos(\omega t)$, and damped by scattering at ion centers, is well approximated by the Drude model. It uses a relaxation time τ_D (or a damping parameter γ_D) independent of ω . In partially ionized systems, or when there are interband effects in solids, it is necessary to include bound-free and bound-bound contributions to $\sigma(\omega)$. A practical extension of the Drude model exploits a model dielectric function. Thus,

$$\begin{aligned} \varepsilon(\omega) &= \varepsilon_r + i4\pi\sigma_r(\omega)/\omega \\ &= 1 - \frac{\omega_{p0}^2}{\omega(\omega + i\gamma_D)} - \sum_{\lambda=1}^{\lambda_m} \frac{\omega_{p\lambda}^2}{\omega(\omega + i\gamma_\lambda) - \varepsilon_\lambda}. \end{aligned} \quad (17)$$

The pure Drude term uses the damping parameter γ_D and a plasma frequency ω_{p0} , while a finite set of oscillators model other processes parametrized by ε_λ , γ_λ , and $\omega_{p\lambda}$. This is useful for fitting experimental data since reflection and transmission experiments could be used to extract best-fit values subject to the sum rule (f -sum rule),

$$\int_0^\infty d\omega \sigma_r(\omega) = \frac{1}{4} \sum_{\lambda=0}^{\lambda_m} \omega_{p\lambda} = \pi n_{\text{tot}} e^2 / m_e. \quad (18)$$

Here n_{tot} involves the free electrons (given by $\bar{Z}\rho$) as well as the electrons occupying the localized atomic states participating in the optical transitions. Thus the mean ionization \bar{Z} , occupation numbers, electron chemical potential μ_e , γ_λ , ε_λ , etc., obtained from the density-functional NPA calculation may be exploited in the fitting process. The simple Drude equation with a *fixed* value of γ_D satisfies the f -sum rule.

If the potential $V_{ie}(q)$ is weak (no bound states), diagrammatic methods can be used. The second-order screened-interaction term is essentially the only one that is tractable in a self-consistent way for realistic potentials. An old result, due to Hopfield, holds if the structure factor is essentially unity [52]. A more complete result, including the contribution from the dynamic structure factor of the ions, can be written down, using an approach similar to that given by Mahan for phonons [53]. Röpke *et al.* have discussed second-order results within the Zubarev approach valid for short-ranged potentials free of bound states [54]. The approach used by Mahan is better adapted for long-range potentials. In fact, even in the two-temperature case where the ions are at a temperature T_i , while the electrons are at a temperature T_e , the Keldysh nonequilibrium propagator technique (assuming that the probe frequency ω does not overlap with core transitions) may be used to show that the frequency-dependent collisional relaxation time $\tau(\omega)$ is [39]

$$\begin{aligned} \tau^{-1}(\omega) &= -(\omega_p^2 \omega)^{-1} \int \frac{q^2 dq M_a^2}{(2\pi)^3} q_z^2 \int \frac{d\nu}{2\pi} \\ &\quad \times \text{Im}[\chi_{ii}(q, \nu)] \text{Im}[\chi_{ee}(q, \nu + \omega)] \Delta N(T_e, T_i, \nu, \omega), \end{aligned} \quad (19)$$

where we have set

$$\Delta N(T_e, T_i, \nu, \omega) = [N\{\beta_e(\nu + \omega)\} - N\{\beta_i(\nu)\}]. \quad (20)$$

Here $N\{\beta_i(\nu)\}$ is a Bose factor giving the occupation number of density-fluctuation modes at the temperature T_i and energy ν . For the equilibrium situation we simply set $T_i = T_e$. Then, as $\omega \rightarrow 0$, this equation can be shown to reduce to the inverse collision time used in the Ziman formula. In Eq. (19), the electron response χ_{ee} and the ion response χ_{ii} mediate the energy and momentum exchange between the two subsystems. The imaginary parts of the response functions are related to the dynamic structure factors by the fluctuation dissipation theorem, which holds for each subsystem at their respective temperatures T_e and T_i [40,55]. We have reproduced this formula here as it links the dynamic and static Ziman calculations with the closely related problems of energy relaxation and two-temperature stationary-state plasmas.

The corrections to the Drude term arising from interband terms in solid aluminum were examined many years ago by Dresselhaus, Harrison, and by Ashcroft and Sturm [48]. They discussed the band-band transitions near ~ 0.05 and 0.15 of the Fermi energy E_F (which is ~ 12 eV for normal density Al). The optical conductivity of normal-density liquid Al slightly above the melting point has been measured by Miller [49] and shows a simple Drude form. A discussion of liquid-metal data including Cu, Ag, and Au is found in Faber [50]. The deviations from the Drude form seen in solid Al arise from the splitting of degenerate bands due to the crystal potential, and to normal interband transitions. Benedict *et al.* have argued that the thermal broadening of the electron self-energy is by itself sufficient to “wash out” these solid-state effects, even if the ion lattice remained intact [51], as may be the case in short-pulse laser generated plasmas. The effect of electron-electron as well as electron-ion interactions on the electron self-energy at finite T was also discussed by us for the hydrogen plasma [35].

The Kohn-Sham eigenvalues of a sample of WDM approximately indicate if the driving field ω could excite bound-bound or bound-free processes. As seen from Table II, the $2p$ levels for the compressed systems ($\kappa=0.5, 1, 2, 4$) range from -4.6 to -2.7 a.u. Hence, the Drude formula would be reasonable for these systems and for standard optical probes since the third term in Eq. (17) may be neglected. However, consider the $\kappa=0.25$ case. Here, in the range $T < 10$ eV, the $2p$ level is ~ -5.5 a.u., but the $3s$ level is very close to the ionization threshold. At $T=8$ eV, the $3s$ level is at -0.165 a.u., and rises to -0.105 a.u. near $T=3$ eV, and then completely disappears for T below ~ 2.5 eV. Since a 300–400 nm optical probe corresponds to about 3–4 eV, bound-free processes would be excited by such probes, deviating from the pure Drude form for the $\kappa=0.25$ case and for more dilute plasmas. When we go to low temperatures, the $\bar{Z}=3$ ionization is very stable, while the $3s$ level creates the presence of $\bar{Z}=1, 2$ ionization states. In the case of $\kappa=0.1$, we have *two* shallow states, viz., $3s$ and $3p$. This finally leads to atomlike photoionization transitions denoted by $3s \rightarrow k$ and $3p \rightarrow k$, where k denotes continuum states (see Fig. 6). The $3p$ photoprocess leads to a strong deviation from the Drude form, and produces a shoulder near

~ 6 eV at $T=10$ in the total absorption. This shoulder moves to lower energies as T is lowered, and finally disappears when T drops below ~ 2.5 eV. Meanwhile the $3s$ level also becomes less bound, while the position of the bound-bound transition ($3s \rightarrow 3p$) undergoes only a modest redshift (Fig. 6), since both $3s$ and $3p$ have shifted.

Much lower densities than the WDM range are probed by Mazevet *et al.* [4], and they identify a sharp signature associated with $3s \rightarrow 3p$ processes near $\omega=5$ eV. In this atomic limit, the pure Drude term is negligible. However, as the ionization increases with increase of density, the Drude term begins to increase, with a resonance at the plasma frequency ω_p which increases with the free-electron density.

A. Dynamic conductivity via the Kubo-Greenwood formula and molecular dynamics

The calculations of Mazevet, Desjarlais *et al.*, and Silvestrelli *et al.* typify [4,11,12,56] the use of molecular dynamics to develop the ionic-liquid structure, while retaining a DFT approach only for the electronic structure. The ion subsystem is modeled with, say, typically 32–256 ions in a simulation box of volume V_b which is periodically repeated. An externally constructed pseudopotential is used. This is not always possible in WDM where several ionic species are present, as in Table I, and an all-electron approach is needed, or the \bar{Z} of the pseudopotential should be bigger than any of the Z_i that may occur. The required number of electrons based on the *assumed ionization model* is placed in the box. The ions are held at some fixed ionic configuration $\{R_i\}$ and the Kohn-Sham electronic wave functions $\psi_f(r, \{R_i\})$ and energies ϵ_f are computed. Given the size of the system, it is not practical to do more than a few k points; usually only one k point, e.g., the Γ point is computed. The conductivity for the given configuration, and for the selected k point with weight $W(\{R_i\}, \vec{k})$, is estimated using the second-order Fermi golden rule formula,

$$\begin{aligned}
 \sigma(\omega, \{R_i\}, \vec{k}) = & \frac{2\pi}{3V_b\omega} \sum_{f_g} W(R_i, \vec{k}) |\langle \psi_f | \vec{p} | \psi_g \rangle|^2 \\
 & \times [n_f(k) - n_g(k)] \delta(\epsilon_f(k) - \epsilon_g(k) - \omega).
 \end{aligned}$$

This is in fact the Kubo-Greenwood (KG) procedure for a crystalline solid. A Kohn-Sham form is used instead of the many-electron eigenstates. The occupation factors $n_f(k)$ are also the one-particle occupations at the appropriate temperature. The energies are the LDA eigenvalues without phonon and other corrections. Similarly, the self-energy effects from the electron-electron processes are also ignored, although they can be quite large [35,51]. Only the *umklapp* processes associated with the reciprocal vectors of the simulation box contribute to the static conductivity. This is because the wave functions are eigenstates of the “crystalline” structure with a “unit cell” of ions at $\{R_i\}$. The actual conductivity has to be obtained by taking a configuration average which requires the Helmholtz free energies for all crystal configurations $\{R_i\}$.

In effect, the method uses simple LDA-DFT for the electrons, but abstains from using DFT for the ions and carries

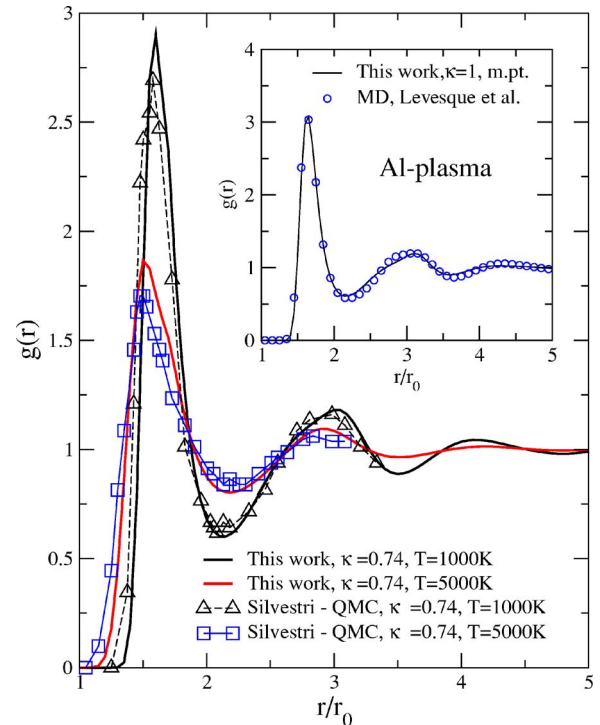


FIG. 5. (Color online) Ion-ion pair-distribution functions of Al from this work compared with the Car-Parinello-type simulations of Silvestrelli [56], labeled QMC. Inset: Comparison at normal density and at the melting point. Here no data from Ref. [56] are available, but we use accurate MD simulations (Levesque *et al.* [57]) for comparison.

out a detailed MD evaluation of the liquid structure. We believe that this is unnecessary if $\omega < \omega_{ip}$, where ω_{ip} is the ion-plasma frequency, since the spherical symmetry of the plasma is a statistically reasonable assumption. The work of Kown *et al.* [14] on strongly coupled H plasmas using these methods and their comparison with our work is an example of this for the static case. In Fig. 5, we compare the ion-ion pair-distribution functions obtained from our NPA+HNC+bridge type procedures with available simulations from Silvestrelli *et al.* [56] and from Levesque *et al.* [57] and show that our effective-one-ion methods recover the multi-ion MD-based $g_{ii}(r)$.

Many of the above mentioned criticisms of the DFT-MD methods, based on the VASP and similar codes, are essentially technical in nature. The method provides an extremely valuable tool, especially important in low-density systems where clustering effects are important and the effective “single-ion” approach of the NPA faces convergence difficulties. It also automatically allows for “ion-microfield” effects via its configuration averaging. However, the DFT-MD approach brings approximations of its own and requires cautious evaluation. An interesting test case would be expanded liquid-Hg [19] using the Kubo-Greenwood MD approach, or the warm-dense Al discussed in Ref. [17] where SESAME [58] tabulations and other approaches become inapplicable. Figure 1 of Ref. [4] considers the Al EOS and confines itself to a region accessible by SESAME. The comparison using the *total pressure* within a log-log plot is unfortunate, since a

TABLE III. Details regarding the $n=3$ shallow states in underdense Al at $T=10$ and 3 eV. Full occupation is when Occ is unity. The ϵ_{3s} and ϵ_{3p} energies are given in Table II. Hartree units are used.

κ	0.25	0.25	0.1	0.1
T	3 eV	10 eV	3 eV	10 eV
μ	0.0393	-0.5538	-0.2029	-0.9589
Occ($3s$)	0.7444	0.2217	0.5806	0.1455
Occ($3p$)			0.1950	0.0843

large part of the total pressure P_T is the ideal pressure P_0 which is common to all models. On the other hand, the excess pressure, $P_{ex}=P_T-P_0$, calculated for Al shows significant deviations in different models [17].

B. Dynamic conductivity from time-dependent density-functional theory

When light shines on a system, the system responds and modifies its level occupations, and creates an internal electric field which modifies the external electromagnetic field. The importance of this type of ‘‘Sternheimer’’ corrections, and the use of time-dependent DFT (TDFT) in predicting absorption cross sections, is well known in calculations for atomic systems [59]. The TDFT formulation relevant to dense plasmas [16] has to include the continuum states, dynamic screening, and coupling to ion dynamics in a computationally convenient, self-consistent manner. However, unlike in atomic systems where line-broadening effects are negligible, the dynamic effects brought in by TDFT have to compete with line-broadening and photoedge smearing arising from plasma collision effects, *unless the TDFT is comprehensive enough to capture all these effects in a self-consistent way*. At the moment we do not have a computationally viable approach which at once includes line broadening, photoedge smearing, ion-dynamical coupling, as well as the TDFT effects associated with the modification of the incoming photon field by the reactive response of the system. Hence we use a phenomenological plasma broadening parameter γ_{ij} for the transition $i \rightarrow j$ and examine the effect of TDFT for a selected case, to assess its importance. In this study, we consider the two cases $\gamma_{ij}=\gamma_D$, i.e., the Drude value, and the case where $\gamma_{ij}=\gamma_0$, with a $\gamma_0 \sim 0.08$ eV, just sufficient to smoothe the numerically produced ripple in the calculated spectra.

The main consequence of the TDFT formulation is to replace, say, the dipole matrix elements $\langle i|\vec{r}|j\rangle$ between states i, j by a dynamic form $\langle i|\vec{r}(\omega)|j\rangle$ where the modification of the driving field by the response of the system is taken into account in a self-consistent manner. Consider a weak external field $\vec{E}_{ext}(t)=\vec{E}\cos(\omega t)$. This corresponds to an external potential,

$$U_{ext}(\vec{r}, t) = e\vec{r} \cdot \vec{E}_{ext}(t). \quad (21)$$

The dipole form of the interaction is used but the momentum or acceleration form of the matrix element may be used when

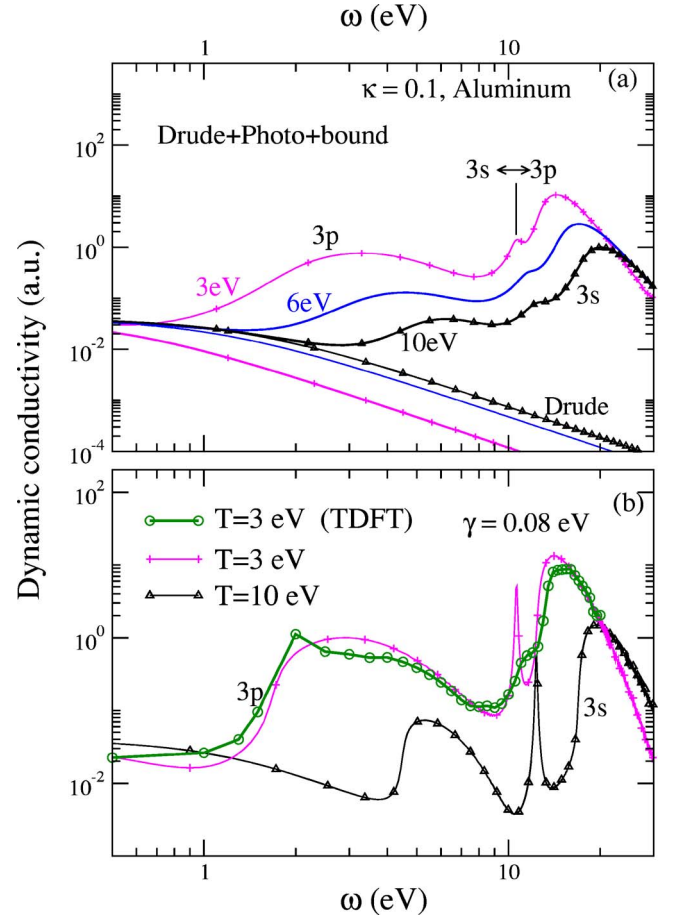


FIG. 6. (Color online) Dynamic conductivity (atomic units) of Al at a compression of 0.1, i.e., 0.27 g/cm^3 at $T=3, 4, 6,$ and 10 eV. Panel (a) shows the Drude conductivity and its modification by the $3s \rightarrow 3p$ bound process and the photoprocesses $3s \rightarrow k$, $3p \rightarrow k$, where k indicates continuum states. The broadening parameter $\gamma=\gamma_D$ is set to the value from the Drude conductivity. Panel (b) uses a fixed minimal broadening γ of ~ 0.08 eV, at $T=3$ and 10 eV. The modification of the $T=3$ eV case when TDFT is used is also shown.

needed. The electric field is directed along the z direction, and we suppress vector notation for the field unless needed. The external potential induces an electron density fluctuation $\delta n(r)$ which generates corrections to the Coulomb and exchange-correlation potentials. Since the linear absorption coefficient (or optical conductivity) is the object of our study, $\delta n(r)$ etc., can be written in terms of the electron response function $\chi^0(r, r'|\omega)$, which can be approximately constructed [16] from the Kohn-Sham eigenstates of the plasma. Then we have

$$U(\vec{r}, \omega) = U_{ext}(\vec{r}, \omega) + V_{ind}^c + V_{ind}^{xc}, \quad (22)$$

$$V_{ind}^c = \int d\vec{r}' \frac{\delta n(\vec{r}, \omega)}{|\vec{r} - \vec{r}'|}, \quad (23)$$

$$V_{ind}^{xc} = \left[\frac{\partial V_{xc}(\vec{r}, \omega)}{\partial n(\vec{r}, \omega)} \right] \delta n(\vec{r}, \omega), \quad (24)$$

$$\delta n(\vec{r}, \omega) = \int d\vec{r}' \chi(\vec{r}, \vec{r}' | \omega) U(\vec{r}', \omega), \quad (25)$$

$$\chi(\vec{r}, \vec{r}' | \omega) = \sum_{ij} \frac{\phi_j^*(r) \phi_i(r) \phi_i^*(r') \phi_j(r') (f_i - f_j)}{\omega + \epsilon_i - \epsilon_j + i\gamma_{ij}}. \quad (26)$$

Here $V_{\text{ind}}^{\text{xc}}(r)$ is calculated from the gradient $\partial V_{\text{xc}} / \partial n$ evaluated at the density $n_0(r)$ in the unperturbed neutral pseudopotential. We use the Kohn-Sham eigenstates $\phi_i(r)$ and the Kohn-Sham eigenvalues ϵ_i , although these should strictly be obtained from a Dyson equation. Since the form of the time-dependent exchange-correlation potential $V_{\text{xc}}(r, \omega)$ is still not established, most implementations use the static $V_{\text{xc}}[n(r)]$ of ordinary density-functional theory. This ‘‘adiabatic’’ approximation works well for discrete spectra, but seems to fail badly for solids and other systems with continuous spectra. Although this is not encouraging for plasmas, we have used the temperature-dependent static $V_{\text{xc}}(n)$ parametrization given in Ref. [29] for these calculations.

The above set of equations have to be solved self-consistently to obtain the total perturbing potential $U(\vec{r}, \omega)$. In effect, the dipole operator, or equivalently, the momentum operator of the scattering electron, is replaced by a space- and time-dependent quantity which enters into the polarizability. Given the spherical symmetry of the system, the total perturbing potential has the form

$$U(\vec{r}, \omega) = -(1/2) E U_\omega(r) Y_1^0(\vec{r}/r). \quad (27)$$

Here Y_1^0 is a spherical harmonic. Also when the transition $\nu \rightarrow \nu' = k, l, m$ and k', l', m' for free-free transitions, the dipole matrix element is replaced by the momentum form, i.e., $|\langle \nu | \vec{r} | \nu' \rangle|^2 = |\langle \nu | \vec{\nabla} | \nu' \rangle|^2 / \omega^2$. In calculating the matrix element $|\langle nlm | r | kl'm' \rangle|^2$, the correct density of states $\aleph(\epsilon)$ for the continuum state $|kl'm'\rangle$, normalized in a sphere of radius R , with $R \rightarrow \infty$, should be included. That is,

$$k_n R - \pi l / 2 = n\pi + \delta_{kl},$$

$$\aleph(\epsilon) = \frac{\partial n}{\partial k} \frac{\partial k}{\partial \epsilon}.$$

The calculations of the matrix elements are very simple if (a) we ignore the Zangwill-Soven type TDFT effects arising from the reaction of the system which act to modify the external field. Then we have the simple Green-Kubo form, (b) if we ignore the phase shifts δ_{kl} of the continuum states, and replace the bound states by hydrogenlike states with the correct $Z = \bar{Z}$. Unfortunately, the final results depend significantly on the assumed line-broadening parameter γ of the transition.

These calculations require the level occupation numbers and the chemical potential, which are significantly different from the free-electron value due to interactions (‘‘continuum lowering’’) [2]. For typical values, see Table III. The effect of level broadening can be included in the above expression by replacing the delta function $\delta(\omega + \epsilon_\nu - k^2/2)$ by a form containing the self-energy corrections to the single-particle levels, as in Grimaldi *et al.*, where self-energies were calcu-

lated. In fact, we have shown in Ref. [35] that the self-energy contribution of ion-electron scattering to level broadening is identical to that given by the Ziman formula. Thus, setting $\gamma = 1/\tau$, we replace the δ function in the above equation with a Lorentzian,

$$\delta(\omega + \epsilon_\nu - k^2/2) \rightarrow \frac{\gamma/\pi}{(\omega + \epsilon_\nu - k^2/2)^2 + \gamma^2}.$$

As already mentioned, we have used $\gamma = \gamma_D$ or a fixed value $\gamma \sim 0.08$ eV.

IV. DISCUSSION

We present results for the dynamic conductivity of some Al plasmas to illustrate the effect of the scattering events where shallow bound states modify the Drude-like conductivity. These ‘‘bound states’’ are really Kohn-Sham eigenvalues and hence their values may need improvement by evaluating the corrections using a Dyson equation [35].

In Fig. 6, we show the conductivity arising from the presence of the $3s$ and $3p$ levels, as well as the Drude term, and the modification when TDFT is included in an approximate manner for the case $T = 3$ eV. Comparison of the upper panel where the plasma broadening term γ_{ij} is set to the value found in the Drude formula, and the lower panel with $\gamma \sim 0.08$ eV, shows that these broadening effects *outweigh* the effects coming from TDFT, at least in this case with $\kappa = 0.1$, $T = 3$ eV. The TDFT spectral intensity of the bound-bound transition is diminished and redistributed, as found in atomic photoemission calculations [59,60]. Some enhancement of the $3p \rightarrow k$ photoedge is also found in this calculation with γ chosen to just smoothe the numerical ripples in the calculation. The broadening γ_{ij} associated with the transition $i \rightarrow j$ includes effects from the ω -dependent electron self-energy and the ion-electron self-energy. The latter depends on the instantaneous ion configuration around the radiator if $\omega > \omega_{ip}$, and hence the NPA model is in serious difficulty since we have used a spherical average in our calculations.

V. CONCLUSION

The first-principles calculation of the dynamic conductivity of warm dense matter may be conveniently carried out within the framework of multicomponent density-functional theory. The static calculation (NPA etc.) provides the Kohn-Sham basis set, phase shifts, pseudopotentials for constructing ion-ion pair potentials, and structure factors. These immediately provide results for the static conductivity which are found to be in good agreement with multi-ion DFT-MD simulations using the VASP code. The ion-ion pair distribution functions are also found to be in good agreement where comparisons are available. Further, the energy levels and occupation numbers obtained from the Kohn-Sham NPA solution can be the starting approximation for a time-dependent density-functional calculation of the optical conductivity. The TDFT results are based on a static exchange-correlation functional, with a fixed plasma broadening γ_0 just enough to smoothe numerical ripples. The calculations with γ

selected according to the Drude value γ_D , which is significantly greater than γ_0 , show that level-broadening effects are strong and have to be self-consistently included in the TDFT calculation—a task *not* achieved here.

ACKNOWLEDGMENTS

The author thanks Dr. François Perrot and Professor Walter Kohn for some of discussions, especially on the role of e - e interactions in conductivity calculations.

-
- [1] F. Perrot and M. W. C. Dharma-wardana, *Phys. Rev. A* **36**, 238 (1987).
- [2] F. Perrot and M. W. C. Dharma-wardana, *Phys. Rev. E* **52**, 5352 (1995).
- [3] F. Perrot, and M. W. C. Dharma-wardana, *Int. J. Thermophys.* **20**, 1299 (1999).
- [4] S. Mazevet, M. P. Desjarlais, L. A. Collins, J. D. Kress, and N. H. Magee, *Phys. Rev. E* **71**, 016409 (2005).
- [5] J. F. Benage, W. R. Shanahan, and M. S. Murillo, *Phys. Rev. Lett.* **83**, 2953 (1999).
- [6] A. W. DeSilva and J. D. Katsouras, *Phys. Rev. E* **57**, 5945 (1998).
- [7] K. Widmann, T. Ao, M. E. Foord, D. F. Price, A. D. Ellis, P. T. Springer, and A. Ng, *Phys. Rev. Lett.* **92**, 125002 (2004).
- [8] C. Niemann, L. Divol, D. H. Froula, G. Gregori, O. Jones, R. K. Kirkwood, A. J. MacKinnon, N. B. Meezan, J. D. Moody, C. Sorce, L. J. Suter, R. Bahr, W. Seka, and S. H. Glenzer, *Phys. Rev. Lett.* **94**, 085005 (2005).
- [9] A. Forsman, A. Ng, G. Chiu, and R. M. More, *Phys. Rev. E* **58**, R1248 (1998).
- [10] A. Ng, T. Ao, F. Perrot, M. W. C. Dharma-wardana, and M. E. Foord, *Lasers Particle Beams* (to be published), e-print arxiv.org/physics/0505070.
- [11] A. Alavi, M. Parrinello, and D. Frenkel, *Science* **269**, 1252 (1995).
- [12] M. P. Desjarlais, *Phys. Rev. B* **68**, 064204 (2003); J. Cl  rouin, P. Renaudin, Y. Laudernet, P. Noiret, and M. P. Desjarlais, *ibid.* **71**, 064203 (2005).
- [13] D. M. Ceperley, *Recent Progress in Many-body Theories*, edited by J. B. Zabolitsky (Springer, Berlin, 1981), p. 262.
- [14] I. Kwon, L. Collins, J. Kress, and N. Troullier, *Phys. Rev. E* **54**, 2844 (1996).
- [15] Y. T. Lee and R. M. More, *Phys. Fluids* **27**, 1273 (1984).
- [16] F. Grimaldi, A. Grimaldi-Lecourt, and M. W. C. Dharma-wardana, *Phys. Rev. A* **32**, 1063 (1985).
- [17] F. Perrot, M. W. C. Dharma-wardana, and J. Benage, *Phys. Rev. E* **65**, 046414 (2002).
- [18] M. W. C. Dharma-wardana and Fran  ois Perrot, *Phys. Rev. B* **66**, 014110 (2002).
- [19] R. N. Bhatt and T. M. Rice, *Phys. Rev. B* **20**, 466 (1979).
- [20] H. Yoneda, H. Morikami, K. I. Ueda, and R. M. More, *Phys. Rev. Lett.* **91**, 075004 (2003).
- [21] Andrew Ng (private communication).
- [22] L. J. Dagens, *J. Phys. (Paris)* **34**, 879 (1973).
- [23] M. W. C. Dharma-wardana and F. Perrot, *Phys. Rev. A* **26**, 2096 (1982).
- [24] F. Perrot, *Phys. Rev. E* **47**, 570 (1993).
- [25] H. Reinholz, R. Redmer, and S. Nagel, *Phys. Rev. E* **52**, 5368 (1995).
- [26] R  pke and H  hne [43] in their appendix have stated similar conclusions.
- [27] S. Kuhlbrodt and R. Redmer, *Phys. Rev. E* **62**, 7191 (2000).
- [28] VASP, <http://cms.mpi.univie.ac.at/vasp/>, M. J. Frisch *et al.*, GAUSSIAN, *Gaussian 98*, Revision A.9 (Gaussian Inc., Pittsburgh, PA, 1998).
- [29] Fran  ois Perrot and M. W. C. Dharma-wardana, *Phys. Rev. B* **62**, 16536 (2000); **67**, 079901(E) (2003).
- [30] A bridge function based on the Yukawa potential may also be used. See W. Daughton, M. S. Murillo, and L. Thode, *Phys. Rev. E* **61**, 2129 (2000).
- [31] <http://babylon.phy.nrc.ca/ims/qp/chandre/> (with password).
- [32] *Density Functional Theory*, edited by E. K. U. Gross and Dreizler, Vol. 337 of NATO Advanced Study Institute Series B: Physics (Plenum, New York, 1993).
- [33] M. P. Surh, T. W. Barbee III, and L. H. Yang, *Phys. Rev. Lett.* **86**, 5958 (2001).
- [34] R. Evans, B. L. Gyorffy, N. Szabo, and J. M. Ziman, in *Properties of Liquid Metals*, edited by S. Takeuchi (Wiley, New York, 1973).
- [35] F. Perrot and M. W. C. Dharma-wardana, *Phys. Rev. A* **29**, 1378 (1984).
- [36] M. W. C. Dharma-wardana, <http://xxx.lanl.gov/cond-mat/0505226>.
- [37] W. W. Schulz and P. B. Allen, *Phys. Rev. B* **52**, 7994 (1995).
- [38] C. Majumdar and W. Kohn, *Phys. Rev.* **138**, A1617 (1965).
- [39] M. W. C. Dharma-wardana and F. Perrot, *Phys. Lett. A* **163**, 223 (1992).
- [40] M. W. C. Dharma-wardana, in *Laser Interactions with Atoms, Solids, and Plasmas*, edited by R. M. More (Plenum, New York, 1994), p. 311.
- [41] L. Spitzer and R. H  rm, *Phys. Rev.* **89**, 977 (1953).
- [42] J. Appel, *Phys. Rev.* **122**, 1760 (1961); **125**, 1815 (1962).
- [43] G. R  pke and F. E. H  hne, *Phys. Status Solidi B* **107**, 603 (1981).
- [44] W. W. Schulz and P. B. Allen, *Phys. Rev. B* **52**, 7994 (1995).
- [45] S. Ethier and J.-P. Matte, *Phys. Plasmas* **8**, 1650 (2001), and references there-in.
- [46] M. B  ttiker, A. Pr  tre, and H. Thomas, *Phys. Rev. Lett.* **70**, 4114 (1993) and references there-in.
- [47] The original Kohn's theorem showed that e - e interactions play no part in cyclotron resonance in uniform systems, while the many generalizations refer to independence from e - e interactions in various properties of uniform and quadratic-confinement systems [e.g., quantum dots, L. Brey, N. F. Johnson, and B. I. Halperin, *Phys. Rev. B* **40**(R), 10647 (1989)].
- [48] N. W. Ashcroft and K. Sturm, *Phys. Rev. B* **3**, 1898 (1971); G Dresselhaus, M. S. Dresselhaus, and D. Beaglehole, as reported in Ashcroft and Sturm.
- [49] J. C. Miller, *Philos. Mag.* **20**, 1115 (1969).
- [50] T. E. Faber, *An Introduction to the Theory of Liquid Metals* (Cambridge University Press, Cambridge, 1972).

- [51] L. X. Benedict, C. D. Spataru, and S. G. Louie, *Phys. Rev. B* **66**, 085116 (2002).
- [52] J. J. Hopfield, *Phys. Rev.* **139**, A419 (1965).
- [53] G. D. Mahan, *J. Phys. Chem. Solids* **31**, 1477 (1970) gives a calculation for phonon scattering.
- [54] G. Röpke, R. Redmer, A. Wierling, and H. Reinholz, *Phys. Rev. E* **60**, R2484 (1999).
- [55] M. W. C. Dharma-wardana and F. Perrot, *Phys. Rev. E* **58**, 3705 (1998); **63**, 069901(E) (2001).
- [56] P. L. Silvestrelli, *Phys. Rev. B* **60**, 16382 (1999); P. L. Silvestrelli, A. Alavi, and M. Parrinello, *ibid.* **55**, 15515 (1997).
- [57] D. Levesque, J. J. Weis, and L. Reatto, *Phys. Rev. Lett.* **54**, 451 (1985); M. W. C. Dharma-wardana and G. C. Aers, *ibid.* **56**, 1211 (1986).
- [58] K. Trainor, in *Handbook of Material Properties Data Bases*, edited by W. Huebner (Los Alamos National Laboratory, Los Alamos, 1948), Vol. Ic, p. 3712.
- [59] A. Zangwill and P. Soven, *Phys. Rev. A* **21**, 1561 (1980).
- [60] F. Perrot and M. W. C. Dharma-wardana, *Phys. Rev. Lett.* **71**, 797 (1993).